Design of an Active Flutter Suppression System

Bradley S. Liebst* and William L. Garrard†
University of Minnesota, Minneapolis, Minnesota
and
William M. Adams‡
NASA Langley Research Center, Hampton, Virginia

An active control law is synthesized for the suppression of wing flutter for a mathematical model of a flight test vehicle. Eigenvalue placement is used to synthesize a full state controller that satisfies performance specifications on control surface activity and that exhibits excellent gain and phase margins. A simple frequency response matching technique is used to design a realizable compensator which approximates the feedback properties of the full state controller. The performance of the control system using this compensator is evaluated at various flight conditions and found to be satisfactory. In addition, eigenvector shaping is used to enhance the gust load alleviation capabilities of the flutter control system.

Nomenclature

Vectors

u	= control input
v_i	= attainable closed-loop eigenvector associated with λ_i eigenvalue
v_i^d	= desired closed-loop eigenvector associated with λ_i eigenvalue
w_i	= vector used in calculation of gain matrix, see Eq. (11)
x	= system state
Γ	= disturbance input vector
ν	= Lagrange multiplier
ξ	= rigid body and flexural generalized coordinates
ξ_c	= control surface displacements

Matrices

$[A_m]$	= aerodynamic coefficient matrix
A	= closed-loop dynamics matrix
B	= control distribution matrix
C	= measurement matrix
$[C_s]$	= structural damping matrix
K	= control gain matrix
$[K_s]$	= structural stiffness matrix
$[M_s]$	= structural mass matrix
N_i	= matrix used in the calculation of w_i, see Eq. (17)
P_i	= eigenvector weighting matrix associated with ith eigenvalue
$[Q_c]$	= unsteady aerodynamic influence coefficient matrix
$[Q_A]$	= s-plane approximation of unsteady aerodynamic influence coefficient matrix
Q,R	= matrices used in eigenvector shaping for uncontrollable modes
V	= matrix whose columns are v_i
W	= matrix whose columns are w_i

Scalars

c	= reference chord, 14 in.
$H(s)G(s)$	= loop transfer function
j	= $\sqrt{-1}$
J_i	= ith adjoined performance index
k	= reduced frequency, $\omega c/2U$
L	= reference length in Dryden gust model, 1700 ft
M	= Mach number
q	= dynamic pressure
s	= Laplace operator
U	= forward velocity
y	= accelerometer output
β_m	= aerodynamic lag frequency
η	= zero mean white noise input to gust model, intensity $(L/U)\bar{\xi}_G^2$
λ_i	= ith eigenvector
ω	= circular frequency
ξ_G	= vertical wind gust velocity
$\bar{\xi}_G$	= rms vertical wind gust velocity
ϕ_i	= influence coefficient associated with acceleration of ith rigid body or flexural mode

Superscripts

d	= desired eigenvector
$*$	= complex conjugate transpose
T	= transpose
-1	= inverse

Subscripts

a	= aileron
e	= elevator
g	= gust
s	= structural

Introduction

ACTIVE suppression of aerodynamic wing flutter can result in substantial weight savings and increases in performance compared with passive methods such as increased structural stiffness and mass balancing.[1] The objective of this paper is to describe the design of an active flutter control system for a mathematical model of a flight test vehicle. Several techniques have been used to design flutter control laws. These include classical feedback control techniques,[2] the aerodynamic energy method of Nissim,[2] linear quadratic Gaussian theory,[3-8] and eigenspace techniques.[8] In this paper an eigenvalue placement is used to design a full state controller

Submitted June 19, 1984; presented as Paper 84-1867 at the AIAA Guidance and Control Conference, Seattle, WA, Aug. 20-22, 1984; revision received March 1, 1985.

*Assistant Professor, Department of Aerospace Engineering and Mechanics. Member AIAA.

†Associate Professor, Department of Aerospace Engineering and Mechanics. Associate Fellow AIAA.

‡Aerospace Technologist, Flight Dynamics and Control Division. Member AIAA.

which is shown to satisfy specifications on rms control surface activity and gain and phase margins over a range of flight conditions. The frequency response characteristics of the full state loop transfer function is approximated by an eighth-order dynamic compensator which converts accelerometer output to control actuator input. In addition, the use of eigenvector shaping to reduce gust loads is examined.

Performance Requirements and System Model

The flight test vehicle considered is a drone with a high-aspect-ratio supercritical wing designed to flutter within the flight envelope. This wing is aerodynamically and structurally similar to those proposed for future air transports. Flutter stabilization is accomplished by the use of small outboard ailerons. Under many flight conditions, the longitudinal rigid body response of the flight test vehicle is unstable. Stabilization of the longitudinal rigid body modes is accomplished by the elevator.

The design flight condition for the flutter control system is a Mach number of 0.86 and an altitude of 15,000 ft (the dynamic pressure at this condition is 4.29 psi). At this flight condition the flutter control sytem is required to stabilize the wing without exceeding specified limits on rms control surface activity. The rms deflection of the outboard aileron is limited to 15 deg and the deflection rate to 740 deg/s. The rms deflection on the elevator is limited to 7 deg and the deflection rate to 80 deg/s. Gain and phase margins of at least 6 dB and 45 deg are required at the design condition.

The aeroelastic model of the wing is given as

$$([M_s]s^2+[C_s]s+[K_s])[\xi]+q[Q_c(s)]\begin{bmatrix}\xi\\ \xi_c\\ \dfrac{\xi_G}{U}\end{bmatrix}=0 \quad (1)$$

$[Q_c(s)]$ is calculated as a function of reduced frequency by a doublet-lattice procedure and is approximated by the matrix of transfer functions

$$[Q_A(s)]=[A_0]+[A_1]\frac{cs}{2U}+[A_2]\left[\frac{cs}{2U}\right]^2+\sum_{m=1}^{L}\frac{[A_{m+2}]s}{s+(2U/c)\beta_m} \quad (2)$$

This approximation has been widely used in design of active flutter suppression systems.[2-8] A single β was used in the design models used in this study.

Three mathematical models were used. Two were design models and one was an evaluation model. The first design model contained three flexural modes plus aerodynamic lag states, aileron actuator dynamics, and a wind gust model. The three flexure modes are shown in Fig. 1. This design model

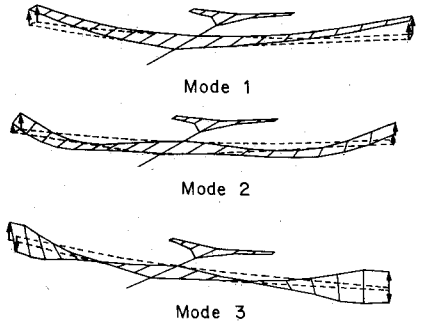

Fig. 1 Flexure modes used in design model.

was 14th order and was used for design of the flutter suppression control laws. The second design model contained the same three flexure modes as the first model, two rigid body modes (plunge and pitch), aerodynamic lag states, aileron and elevator actuator dynamics, and a wind gust model. This design model was 21st order and was used for the synthesis of the combined flutter suppression/gust load alleviation control laws. The evaluation model contained two rigid body modes and ten flexure modes, aileron and elevator actuator dynamics, a gust model, and a doublet-lattice model of the unsteady aerodynamics. This model was 28th order.

In the design models, the lowest-frequency flexural mode is first-mode bending, the next highest is second-mode bending, and the highest is first-mode torsion. First-mode bending is the unstable mode; whereas second-mode damping increases with velocity. The frequencies of these two modes approach one another as velocity increases. At an altitude of 15,000 ft, the wing flutters at approximately $M=0.75$. The locus of the open-loop aeroelastic roots with increasing dynamic pressure is shown in Fig. 2.

A second-order Dryden vertical wind gust model

$$\xi_G(s)/\eta(s)=[1+(\sqrt{3}L/U)s]/[1+(L/U)s]^2 \quad (3)$$

is used. The rms gust velocity is 12 ft/s.

The aileron/actuator transfer function is

$$\xi_{c_a}(s)/u_a(s)=1.7744728\times10^7/(s+180)[s^2+251s+(314)^2] \quad (4)$$

and the elevator/actuator transfer function is

$$\xi_{c_e}/u_e=20/(s+20) \quad (5)$$

Equations (1-5) can be combined to give the design model for the wing, control surfaces and actuators, and wind gust in vector-matrix form as

$$\dot{x}=Ax+Bu+\Gamma\eta \quad (6)$$

The motion of the wing is sensed by a pair of accelerometers mounted forward and inboard of the control surface on each wing. The combined scalar output of each accelerometer pair

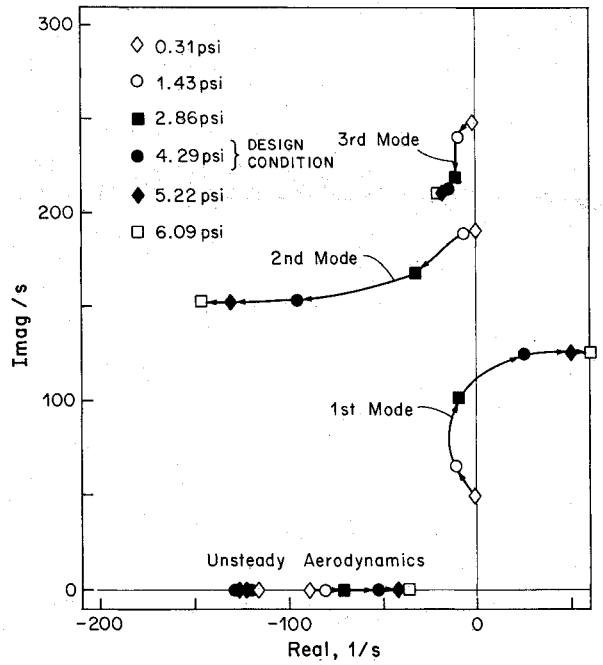

Fig. 2 Locus of open-loop aeroelastic eigenvalues as a function of dynamic pressure.

is

$$y = \sum_{i=1}^{n} \phi_i \ddot{\xi}_i = Cx \tag{7}$$

Theory of Eigenspace Design

Moore[9] and others have shown how feedback can be used to directly place closed-loop eigenvalues and also to shape closed-loop eigenvectors. If performance specifications are given or can be interpreted in terms of desired closed-loop eigenvalues and eigenvectors, then these techniques can provide a natural design procedure where the desired eigenstructure (if obtainable) can be calculated without iteration. This has been successfully demonstrated by Cunningham,[10] Andry et al.,[11] and Sobel and Shapiro[12] in decoupling aircraft rigid body modes. If performance specifications cannot be clearly stated in terms of closed-loop eigenvalues and eigenvectors—for example, specifications on rms responses and/or stability margins—it may be necessary to iterate eigenvalues and/or eigenvectors until performance specifications are met.[8,12]

Some basic results for eigenspace design for controllable and observable systems are briefly summarized below. More detailed discussions can be found in Refs. 9-11. Consider a system described by equations of the form of Eqs. (6) and (7) with a linear control law

$$u = Ky \tag{8}$$

where $\dim(x) = n$, $\dim(u) = m$, and $\dim(y) = r$. If the system is controllable and observable and the matrices B and C are full rank, the following four results can be proven.

1) The position of a total of m or r (whichever is greater) closed-loop eigenvalues can be arbitrarily assigned with the normal stipulation that, if λ_i is a complex closed-loop eigenvalue, its complex conjugate λ_i^* must also be a closed-loop eigenvalue.

2) The shape of the eigenvectors associated with these eigenvalues can be altered. If the shape of a complex closed-loop eigenvector v_i is altered, its complex conjugate v_i^* must be altered in the same way.

3) A total of m or r (whichever is smaller) elements of each eigenvector that can be altered can be chosen arbitrarily.

4) The eigenvector associated with the closed-loop eigenvector λ_i must lie in the subspace spanned by $(I\lambda_i - A)^{-1}B$.

Conditions 1 and 2 do not preclude using feedback to change real open-loop eigenvalues to compex closed-loop eigenvalues or vice versa.

If it is desired to move an eigenvalue, the design procedure consists of determining a gain matrix K such that for all desired closed-loop eigenvalue (λ_i) and eigenvector (v_i) pairs

$$(A + BKC)v_i = \lambda_i v_i \tag{9}$$

This is equivalent to finding w_i such that

$$(\lambda_i I - A)v_i = Bw_i \tag{10}$$

Once the w_is have been found, the gain matrix is calculated as

$$K = W[CV]^{-1} \tag{11}$$

Since the desired eigenvectors are in general not achievable, the w_is are selected to minimize the weighted sum of the squares of the difference between the elements of the desired and attainable eigenvector as given by the following performance index

$$J_i = (v_i - v_i^d)^* P_i (v_i - v_i^d) \tag{12}$$

where P_i is a positive definite symmetric matrix whose elements can be chosen to weight the difference between certain elements of the desired and attainable eigenvectors more heavily than others. Earlier work by the authors and others[8-11] has required that controllable eigenvalues must be moved if the corresponding eigenvectors were to be altered. The present method relaxes that requirement. For a fixed λ_i, it is desired to minimize J_i subject to Eq. (10). Adjoining Eq. (10) to J_i with Lagrange multipliers ν_i, we get

$$\bar{J}_i = \tfrac{1}{2}(v_i - v_i^d)^* P_i (v_i - v_i^d) + \nu_i^* [(I\lambda_i - A)v_i - Bw_i] \tag{13}$$

J_i is minimized when

$$\frac{\partial \bar{J}_i}{\partial w_i} = 0 = -\nu^* B \tag{14}$$

$$\frac{\partial \bar{J}_i}{\partial v_i} = 0 = (v_i - v_i^d)^* P_i + \nu^* (I\lambda_i - A) \tag{15}$$

In matrix form, Eq. (10), (14), and (15) are

$$\begin{bmatrix} (I\lambda_i - A) & -B & 0 \\ 0 & 0 & B^T \\ P_i & 0 & (I\lambda_i - A)^* \end{bmatrix} \begin{Bmatrix} v_i \\ w_i \\ \nu_i \end{Bmatrix} = \begin{Bmatrix} 0 \\ 0 \\ P_i v_i^d \end{Bmatrix} \tag{16}$$

or

$$N_i \begin{Bmatrix} v_i \\ w_i \\ \nu_i \end{Bmatrix} = \begin{Bmatrix} 0 \\ 0 \\ P_i v_i^d \end{Bmatrix} \tag{17}$$

As shown in the Appendix, if the system is controllable, N_i is nonsingular even if λ_i is not moved from its open-loop value. The attainable v_i and w_i are then

$$\begin{Bmatrix} v_i \\ w_i \\ \nu_i \end{Bmatrix} = N_i^{-1} \begin{Bmatrix} 0 \\ 0 \\ P_i v_i^d \end{Bmatrix} \tag{18}$$

If an eigensolution is not to be altered, setting $w_i = 0$ assures that the associated v_i and λ_i remain in their open-loop configuration. Also, in case of complex eigenvalues, a real gain matrix can be obtained from a simple transformation.[9]

The algorithm given above fails for an uncontrollable eigenvalue (the gust eigenvalues in the present problem) λ_g because N_g is singular. This problem can be solved by partitioning the eigenvector v_g associated with the eigenvalue λ_g as shown below. Partition v_g such that

$$[I\lambda_g - A]v_g = Bw_g \tag{19}$$

becomes

$$\left[\begin{array}{c|c} (I\lambda_g - A^I) & Q \\ \hline 0 & R \end{array}\right] \left[\begin{array}{c} v_g^I \\ \hline v_g^{II} \end{array}\right] = \left[\begin{array}{c} B^I \\ \hline 0 \end{array}\right] w_g \tag{20}$$

where v_g^{II} contains only uncontrollable states. The equation

$$Rv_g^{II} = 0 \tag{21}$$

is automatically satisfied if v_g^{II} is selected to be equal to the open-loop portion of v_g, which contains the uncontrollable states. Since λ_g is not an eigenvalue of A^I, $[I\lambda_g - A^I]$ is nonsingular and by performing the indicated calculations, w_g and v_g^I can be determined in much the same way as for the controllable eigenvalues. Minimization of

$$J_g = (v_g^I - v_g^{Id})^* P_g (v_g^I - v_g^{Id}) \tag{22}$$

subject to

$$(I\lambda_g - A^I)v_g^I + Qv_g^{II} = B^I w_g \tag{23}$$

yields

$$\begin{Bmatrix} v_g^I \\ w_g \\ v_g \end{Bmatrix} = N_g^{-1} \begin{Bmatrix} -Qv_g^{II} \\ 0 \\ P_g v_g^{Id} \end{Bmatrix} \tag{24}$$

where

$$N_g = \begin{bmatrix} (I\lambda_g - A^I) & -B^I & 0 \\ 0 & 0 & B^{IT} \\ P_g & 0 & (I\lambda_g - A^I)^* \end{bmatrix} \tag{25}$$

Once all w_i's and v_i's have been calculated, the gain matrix is determined from Eq. (11).

Full-State Flutter Suppression Control Law Synthesis

The full state flutter control law was designed by rotating the unstable eigenvalues about the imaginary axis and maintaining all other eigensolutions in their open-loop configuration. Since a single control surface, the outboard aileron, was used, it was only possible to place controllable eigenvalues and shape eigenvectors associated with the uncontrollable (gust) eigenvalues. It was found that moving the gust eigenvectors from their open-loop configurations resulted in large increases in control surface activity; therefore, these eigenvectors were maintained in their open-loop configuration. The locus of the closed-loop aeroelastic roots with increasing dynamic pressure is shown in Fig. 3. The wing with active flutter suppression becomes unstable at about 5.30 psi whereas, from Fig. 2, the open-loop wing becomes unstable at about 3.0 psi. This corresponds to a 65% increase in flutter dynamic pressure or a 28% increase in flutter speed if air density remains constant. The rms aileron activity as detemined from the design model is shown in Table 1 for various values of dynamic pressure. It can be seen that the maximum allowable values of 15 deg and 740 deg/s are not exceeded.

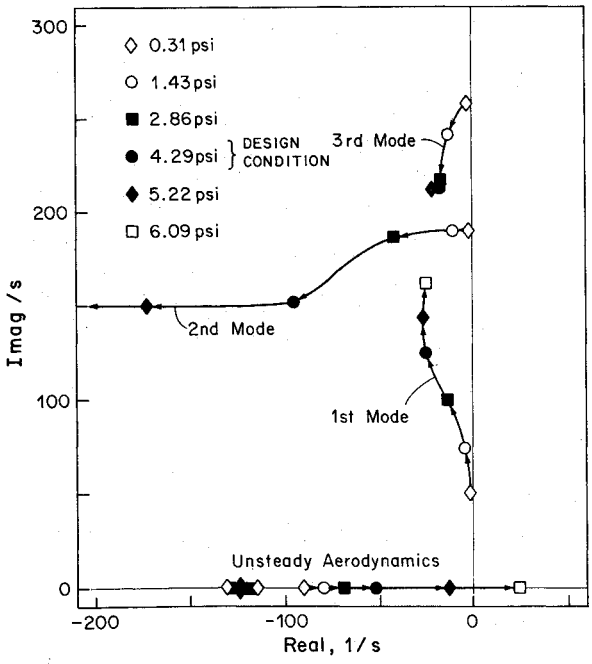

Fig. 3 Locus of closed-loop (full-state) aeroelastic eigenvalues as a function of dynamic pressure.

The loop transfer function for the system at the design condition is given below:

$$H(s)G(s) = K(Is - A)^{-1}B = \frac{-99.6(s - 0.103)}{[s^2 - 49.8s + (126.7)^2]} \tag{26}$$

Note that since $u = +Kx$ the characteristic equation is given by

$$1 - H(s)G(s) = 0 \tag{27}$$

and the critical condition for stability occurs when the phase angle of $H(j\omega)G(j\omega)$ equals zero. Bode diagrams for the full state controller at $M = 0.86$ and 15,000 ft (the design condition) are shown in Figs. 4 and 5. Gain margin is 6 dB and phase margins are ± 60 deg. At a dynamic pressure of 2.8 psi, corresponding to $M = 0.7$, gain margins are infinite, and phase margins are 180 and 90 deg. It is unlikely that the flutter controller would be operational at dynamic pressures lower than 2.85 psi; therefore, the full state controller exhibits excellent stability margins over its operating range.

Frequency Domain Compensator Design

The transfer function between the outboard aileron control input and the wing accelerometer output is

$$y(s)/u_a(s) = C[Is - A]^{-1}B = G_a(s) \tag{28}$$

At the design condition,

$$G_a(s) = \frac{1.78108 \times 10^5 (s^2 + .488s + 1.248)(s + 6290)}{(s + 180)[s^2 + 251s + (314)^2][s^2 + 197.8s + (183)^2]}$$

$$\times \frac{(s - 0.877)(s + 1.43)[s^2 + 69.8s + (104.2)^2]}{[s^2 - 49.8s + (126.7)^2](s + .52)^2} \tag{29}$$

in units of g/deg of control surface displacement. Although the design model is 14th order, the third flexural mode and the three aerodynamic lag states are for all practical purposes canceled by zeros in the numerator and the open-loop transfer function is ninth order.

It was possible to develop a dynamic compensator

$$u(s)/y(s) = H_c(s) \tag{30}$$

which resulted in approximately the same feedback properties as the full state controller. In previous studies $H(s)$ has been designed using Kalman filters with robustness properties enhanced by the Doyle-Stein procedure[4-7,14,15] and by frequency response matching.[3] In frequency response matching, $H_c(s)$ is selected so that

$$H_c(s)G_a(s) \approx H(s)G(s) \tag{31}$$

over a frequency range of interest. The following compensator transfer function was synthesized to satisfy this requirement by letting $H_c(s) \approx H(s)G(s)G_a^{-1}(s)$. The compensator

Table 1 RMS aileron deflection and deflection rate for various dynamic pressures for 12 ft/s gust

Dynamic pressure, psi	RMS deflection, deg	RMS deflection rate, deg/s
1.43	10.0	244.6
2.86	5.3	273.0
4.29	2.0	259.0
5.22	2.1	265.6

transfer function is

$$H_c(s) = \frac{-1.61039\times 10^4(s+180)[s^2+251s+(314)^2]}{(s+6290)[s^2+69.8s+(104.2)^2](s^2+.488s+1.248)}$$

$$\times\frac{[s^2+197.8s+(183)^2](s+.52)^2}{(s+1.43)(s+5000)^2} \quad (32)$$

The units of $H_c(s)$ are deg/g. All the poles and zeros of $G_a(s)$ except for the poles at $24.9\pm j124.4$ and the zero at 0.877 are canceled. It was necessary to retain the unstable poles to approximate $H(s)G(s)$ and, since a stable compensator was desired, the right half-plane zero was not canceled. Two compensator poles were added at -5000 in order to provide high-frequency rolloff. The overall gain of H_c was adjusted so that $H_c(s)G_a(s)$ matched $H(s)G(s)$ at the frequency at which $H(s)G(s)$ was a maximum.

The resulting loop transfer function at the design flight condition of $M=0.86$ and 15,000 ft was

$$H_c(s)G_a(s)\frac{-2.868\times 10^9(s-.877)}{[s^2-49.8s+(126.7)^2](s+5000)^2} \quad (33)$$

Bode diagrams of $H_c(s)G_a(s)$ at this flight condition are shown in Figs. 4 and 5. It can be seen that $H(s)G(s)$ is approximated very closely in the frequency range shown. $H_c(s)G_a(s)$ has 180 deg more phase lag at high frequencies than does $H(s)G(s)$, but at these frequencies $H_c(s)G_a(s)$ has rolled off sufficiently so that this is not a problem. As shown in Table 2, the design model showed rms responses very close to those for the full state controller. Sensor noise equal to accelerometer errors of 2% and 20% was simulated. Accelerometer bandwidth was 10,000 Hz. The 2% and 20% was simulated. Accelerometer bandwidth was 10,000 Hz. The 2% error produced essentially the same results as for no sensor noise while a 20% error produced only small increases in rms control deflection and deflection rate. Since accelerometer noise is estimated to be in the 2% range, sensor noise rejection appears to be excellent.

Table 2 Results for $M=0.86$ and $h=15{,}000$ ft design model

Controller	Aileron deflection, deg	Aileron rate, deg/s	Gain Margin, dB	Phase margin, deg
Full state	2.0	259.0	6.0	±60
Compensator without sensor noise	2.72	250.8	6.0	±60
Compensator with sensor noise	2.75	251.5	6.0	±60

The performance of this compensator was determined at the design flight condition using an evaluation model that included two rigid body modes and ten flexural modes. The unsteady aerodynamics were taken directly from the doublet-lattice calculations rather than the Laplace transform approximations used in the design model. Both Dryden and von Kármán gust models were used. As suggested in Ref. 16, a characteristic length of 1700 ft was used with the Dryden model and a characteristic length of 2500 ft was used with the von Kármán model. The results are summarized in Table 3. Rms responses increased when compared with the design model but were still within acceptable bounds. Gain and phase margins decreased somewhat but were still acceptable. Increasing the compensator gain to restore the gain margin to 6 dB resulted in slightly improved performance.

At a dynamic pressure equivalent to Mach 0.7 at 15,000 ft, the phase angle never passes through zero degrees, and gain margins are infinite. Phase margins are 118 and 79 deg. Thus, this compensator shows very good stability margins over the range of dynamic pressure where the flutter control system is to be operated.

Eigenvector Shaping for Gust Load Reduction

Since the controllers described previously use a single control surface, shaping of eigenvectors associated with controllable eigenvalues is impossible. In order to examine the ability of eigenvector shaping to improve performance, rigid body modes and the elevator were added to the design model. It was decided to see if eigenvector shaping could be used to reduce gust loads at the flutter condition. Since the rigid body and first flexural modes were unstable at this flight condition, it was necessary to stabilize all of these modes. A baseline case was generated by first using eigenvalue placement in conjunction with the elevator to move the rigid body eigenvalues from $-3.10\pm j5.84$, 8.9, and 0 to $-4\pm j4$, -0.01, and -0.015. A

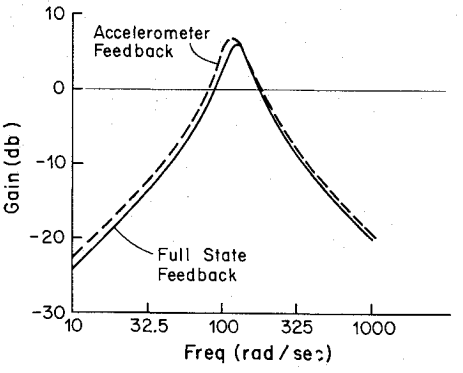

Fig. 4 Log gain of $H(s)G(s)$ vs frequency for $M=0.86$ for full state and accelerometer feedback.

Table 3 Results of dynamic compensator evaluated using 10 flexure states and 2 rigid body states and doublet lattice aerodynamics

	Outboard aileron		Elevator			
	Deflection deg	Deflection rate, deg/s	Deflection, deg	Deflection rate, deg/s	Gain margin, dB	Phase margin, deg
Nominal compensator						48.55 @ 169 rad/s
(von Kármán)	5.51	627	0.106	0.525	4.87 @	48.00 @
(Dryden)	3.47	385	0.188	0.446	138 rad/s	93.9 rad/s
Compensator with gain increased						52.6 @ 177 rad/s
					6.09 @	52.3 @
(von Kármán)	5.46	612	0.106	0.521	138.4 rad/s	91.5 rad/s
(Dryden)	3.46	376	0.119	0.445		

new A matrix was then generated using the closed-loop control laws for stabilization of the rigid body modes. Next, a flutter controller was designed as before by rotating the unstable eigenvalues about the imaginary axis and keeping all other eigensolutions in their previous positions. Thus, although two controls were available, controller synthesis was treated as two sequential problems each, in which only a single control was available and eigenvector shaping could not be performed. The rms control surface deflections and rates and the root bending moment, shear, and torque are given in Table 4. The aileron deflection and deflection rate are different from the values given earlier because of the addition of the rigid body modes.

Additional designs were then performed using both controls simultaneously so that eigenvector shaping was possible. The first flexure mode displacement has by far the largest influence on wing root loads. Thus, it was decided to try and reduce the magnitude of wing root loads by driving the first mode components of all eigenvectors to zero. Since only the eigenvalues associated with the rigid body and first flexure modes were moved from their open-loop positions, the method developed for shaping eigenvectors without moving associated eigenvalues described in the section Theory of Eigenspace Design was used to shape 15 of the 21 system eigenvectors. Values of the weighting terms on the squares of the difference between the components of the desired and attainable eigenvectors in the direction of the first flexure mode were varied from 0.001 to 500.0, while the other weighting terms were unity. The best results in terms of rms control surface and wing root loads were obtained for weighting factors of 0.85. These results are shown in Table 5. Compared with the baseline control system aileron deflection, deflection rate and elevator rate increase somewhat; however, elevator displacement decreases substantially. Wing root bending moment, shear, and torque are 84, 89, and 74%, respectively, of their baseline values. An attempt to improve performance further by reducing both first and second flexure mode displacement did reduce loads compared with the baseline case; however, reductions in loads were not as great as when only reduction of first mode displacement was attempted (see Table 5).

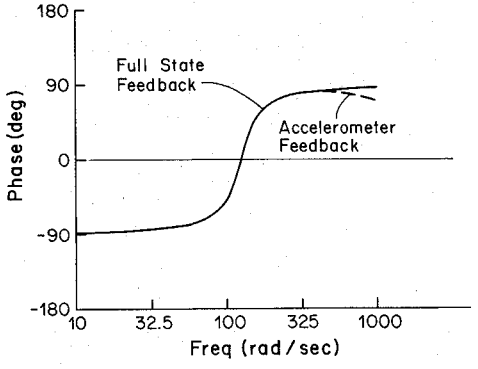

Fig. 5 Phase of $H(s)G(s)$ vs frequency for $M=0.86$ for full-state and accelerometer feedback.

Next, the rigid body pitch (or short period) eigenvalues were varied from $-2\pm j2$ to $-7\pm j7$ using the desired eigenvector set used for the reduction of the first mode displacement. This was done to see what effect changing the eigenvalues associated with the pitching mode would have on the wing root loads. The results are shown in Table 4. Reducing pitch frequency reduces bending moment and shear but increases torque and control surface activity. Increasing pitch frequency increases elevator activity and torque and decreases aileron activity, bending moment, and shear slightly.

Since there are two control surfaces, the stability margins of the baseline and best gust load alleviation control laws were evaluated using the minimum singular value of the return difference matrix $I-H(s)G(s)$.[15,17,18] At low frequencies the plunge (or phugoid) roots located near the imaginary axis resulted in poor stability margins for both designs; however, these margins should not be a problem since in a piloted aircraft a mildly unstable phugoid mode is acceptable and in an unpiloted aircraft an outer loop controller (autopilot) would be used to maintain desired altitude and compensate for low-frequency instabilities. The stability margins in the range of fequencies near flutter are of critical importance. In this range, the baseline design has a minimum singular value of 0.931 at a frequency of 130 rad/s. This corresponds to gain margins of -5.7 and 53.5 dB with no variations in phase and phase margins of ± 55.5 deg with no variations in gain (these are analogous to classical gain and phase margins for single-input, single-output systems).[17,18] The best gust load alleviation design has a minimum singular value fo 0.605 at 130 rad/s; this corresponds to gain margins of -4.1 and 8.1 dB with no variations in phase and phase margins of ± 35.2 deg with no variation in gain. Thus, it can be seen that shaping the eigenvectors to achieve improved gust load alleviation results in some degradation in stability margins.

Conclusions

A feedback system designed on the basis of a model containing three structural modes appears to satisfy the performance requirements for the flutter controller in terms of rms control surface activity and stability margins. The controller is designed by using eigenspace techniques to rotate the unstable flutter eigenvalues about the imaginary axis and leave all other eigensolutions in their open-loop positions. The resulting full state control law can be approximated from a single accelerometer output by using a dynamic compensator that approximates the full state loop transfer function.

Table 4 Performance results for combined elevator/aileron control, $M=0.86$, $h=15{,}000$ ft, 12 ft/s gust

Control design	Elevator disp, deg	Elevator rate, deg/s	Aileron disp, deg	Aileron rate, deg/s	Wing root bending moment, $\times 10^4$ in.-lb	Wing root shear, $\times 10^2$ lb	Wing root torque, $\times 10^3$ in.-lb
Baseline	6.10	2.29	1.87	251.8	1.708	2.871	1.374
Reduction of 1st mode disp.	2.22	8.00	3.22	264.0	1.428	2.551	1.009
Reduction of 1st & 2nd mode disp.	2.27	6.86	3.27	263.6	1.436	2.565	1.031
Pitch eigenvalues $-2\pm j2$	3.539	21.32	12.04	351.4	0.829	0.843	2.219
Pitch eigenvalues $-7\pm j7$	3.165	9.525	2.79	255.2	1.34	2.358	1.089

A method for shaping eigenvectors associated with uncontrollable eigenvalues and with controllable open-loop eigenvalues that are not moved was developed and used to enhance the gust load alleviation characteristics of the flutter controller. Improvement in gust load alleviation was acheived at the expense of reduced stability margins.

Appendix

The $(2n+m)$ by $(2n+m)$ matrix

$$N_i=\begin{bmatrix} (I\lambda_i-A) & -B & 0 \\ 0 & 0 & B^T \\ P_i & 0 & (I\lambda_i-A)^* \end{bmatrix}$$

is shown to be nonsingular as follows. First, consider the state equation transformed into diagonal form

$$\dot{x}=\Lambda x+Bu \qquad \Lambda=\begin{bmatrix} \lambda_1 & & 0 \\ & \lambda_2 & \\ 0 & & \ddots \end{bmatrix} \qquad \text{Then} \qquad I\lambda_i-\Lambda=\begin{bmatrix} (\lambda_i-\lambda_1) & & 0 \\ & (\lambda_i-\lambda_2) & \\ 0 & & \ddots \end{bmatrix}$$

Now, assume the eigenvector or weighting matrix P_i is diagonal, then N_i becomes

$$\begin{array}{l} \text{rows 1 to } n \\ N_i=\text{rows } n+1 \text{ to } n+m \\ \text{rows } n+m+1 \text{ to } 2n+m \end{array} \begin{bmatrix} (\lambda_i-\lambda_1) & \cdots & 0 & -b_{11} & \cdots & -b_{1m} & 0 & \cdots & 0 \\ \vdots & & \vdots & \vdots & & \vdots & \vdots & & \vdots \\ 0 & \cdots & (\lambda_i-\lambda_n) & -b_{n1} & \cdots & -b_{nm} & 0 & \cdots & 0 \\ 0 & \cdots & 0 & 0 & \cdots & 0 & b_{11} & \cdots & b_{n1} \\ \vdots & & \vdots & \vdots & & \vdots & \vdots & & \vdots \\ 0 & \cdots & 0 & 0 & \cdots & 0 & b_{1m} & \cdots & b_{nm} \\ P_1 & \cdots & 0 & 0 & \cdots & 0 & (\lambda_i-\lambda_1)^* & \cdots & 0 \\ \vdots & & \vdots & \vdots & & \vdots & \vdots & & \vdots \\ 0 & \cdots & P_n & 0 & \cdots & 0 & 0 & \cdots & (\lambda_i-\lambda_n)^* \end{bmatrix}$$

To prove that N_i is nonsingular, we need only prove N_i has rank $2n+m$ or that all possible sums of multiples of rows will not result in a zero row. If we have a controllable system the first $n+m$ rows have rank $n+m$ for all values of the desired eigenvalue λ_i. Since P_i is positive definite, the last n rows have rank n. Last, if P_i is positive definite the last n rows could never cancel the first $n+m$ rows and vice versa.

If the system is uncontrollable, transforming it to the controllability canonical form would easily show that the first $n+m$ rows would not have rank $n+m$ when λ_i was one of the uncontrollable eigenvalues.

Acknowledgments

The research reported in this paper was supported by NASA Langley Research Center under Grant NAG-1-217. Mr. Craig McCarty, a graduate student at the University of Minnesota, assisted in performing many of the calculations.

References

[1]Shomber, A., "Application of Integrated Active Controls to Future Transports," AIAA Paper 79-1654, *Proceedings of 1979 Guidance and Control Conference,* Aug. 1979.

[2]Abel, I., Newsom, J.R., and Dunn, H.J., "Application of Two Synthesis Methods for Active Flutter Suppression of an Aeroelastic Wind Tunnel Model," AIAA Paper 79-1633, Aug. 1979.

[3]Newsom, J.R., "Control Law Synthesis for Active Flutter Suppression Using Optimal Control Theory," *Journal of Guidance and Control,* Vol. 2, Sept.-Oct. 1979, pp. 388-394.

[4]Mahesh, J.K., Stone, C.R., Garrard, W.L., and Dunn, H.J., "Control Law Synthesis for Flutter Suppression Using Linear Quadratic Gaussian Control Theory," *Journal of Guidance and Control,* Vol. 4, July-Aug. 1981, pp. 415-422.

[5]Mukhopadhyay, V., Newsom, J.R., and Abel, I., "Reduced Order Optimal Feedback Control Law Synthesis for Flutter Suppression," *Journal of Guidance and Control,* Vol. 4, July-Aug. 1981, pp. 382-395.

[6]Newsom, J.R., "Design of the Flutter Suppression System for a Remotely Piloted Research Vehicle (DAST ARW-1R)," AIAA Paper 83-0990-CP, *Proceedings of the AIAA/ASME/ASCE/AHS Structures, Structural Dynamics and Materials Conference,* May 1983.

[7]Adams, W.M. and Tiffany, S.H., "Design of a Candidate Flutter Suppression Control Law for the DAST ARW-2," NASA TM 86257, July 1984.

[8]Garrard, W.L. and Liebst, B.S., "Active Flutter Suppression Using Eigenspace and Linear Quadratic Design Techniques," *Journal of Guidance, Control, and Dynamics,* Vol. 8, May-June 1985, pp. 304-311.

[9]Moore, B.C., "On the Flexibility Offered by Full State Feedback in Multivariable Systems Beyond Closed Loop Eigenvalue Assignment," *IEEE Transactions on Automatic Control,* Vol. 21, Oct. 1976, pp. 682-691.

[10]Cunningham, Thomas B., "Eigenspace Selection Procedures for Closed Loop Response Shaping with Modal Control," *Proceedings of IEEE Conference on Decision and Control,* Dec. 1980.

[11]Andry, A.N., Shapiro, E.Y., and Chung, J.C., "On Eigenstructure Assignment for Linear Systems," *IEEE Transactions on Aerospace and Electronic Systems,* Sept. 1983.

[12]Sobel, K.M. and Shapiro, E.Y., "A Design Methodology for Pitch Pointing Flight Control Systems," *Journal of Guidance, Control, and Dynamics,* Vol. 8, March-April 1985, pp. 181-187.

[13]Safanov, M.G. and Athans, M., "Gain and Phase Margins of Multi-Loop LQG Regulators," *IEEE Transactions on Automatic Control,* Vol. 22, April 1977, pp. 173-179.

[14]Garrard, W.L., Mahesh, J.K., Stone, C.R., and Dunn, H.J., "Robust Kalman Filter Design for Active Flutter Suppression Systems," *Journal of Guidance, Control, and Dynamics,* Vol. 5, July-Aug. 1982, pp. 412-414.

[15]Doyle, J.C. and Stein, G., "Multivariable Feedback Design: Concepts for a Classical/Modern Synthesis," *IEEE Transactions on Automatic Control,* Vol. 26, Feb. 1981, pp. 4-16.

[16]Chalk, C.R. et al., *Background Information and Users Guide for MIL-F-8785B(ASG), Military Specifications of Piloted Airplanes,* AFFDL-TR-69-72, Aug. 1969.

[17]Lehtomaki, N.A., Sandell, R., and Athans, M., "Robustness Results in Linear Quadratic Based Multivariable Control Designs," *IEEE Transactions on Automatic Control,* Vol. 26, Feb. 1981, pp. 75-92.

[18]Mukhopadhyay, V. and Newsom, J.R., "A Multiloop System Stability Margin Study Using Matrix Singular Values," *Journal of Guidance, Control, and Dynamics,* Sept.-Oct. 1984, pp. 582-587.